Optimization of novel thermo-gelling tri-block co-polymeric carriers for the delivery of paclitaxel for the treatment glioblastoma multiforme

Honors Thesis

Presented to the College of Agriculture and Life Sciences, Biological Sciences Program

Of Cornell University

In Partial Fulfillment of the Requirements for the

Research Honors Program

By

Cody D. Schlaff

May 2011

Dr. Michael L. Shuler, Dr. Alexis J. Torres and Dr. Susan C. Pannullo

Department of Biomedical Engineering, Cornell University

Department of Neurological Surgery, Weill Cornell Medical College

ABSTRACT

Glioblastoma multiforme (GBM) is the most aggressive primary brain cancer in adults and unfortunately, characterized by a poor prognosis. Standard treatments like surgical resection and chemotherapy are marginally effective. Despite aggressive therapy, the disease ultimately recurs. Local control-released chemotherapy may be administered via carmustine (BCNU) polymer-loaded biodegradable wafers (Gliadel® wafers) to the cavity upon surgical resection. One significant limitation of this modality is the instability of BCNU in aqueous media. Moreover, the effective therapeutic distance of the wafers extends only a few millimeters from the resection cavity, while recurrences occur often centimeters away. New carriers and pharmacological agents are being actively explored. One such carrier is derived from a novel set of poly(DL-lactide-co-glycolide-b–ethylene glycol-b-DL-lactide-co-glycolide) (PLGA-PEG-PLGA) thermo-gelling tri-block copolymers capable of sustained release of paclitaxel. Paclitaxel has been shown *in vitro* and *in vivo* to be effective against glioma cells while having a much slower degradation rate than carmustine; this slower degradation may allow deeper penetration into the brain than BCNU and an effective concentration that can be sustained for a longer period. We seek to test whether thermo-gelling hydrogel carriers of paclitaxel could result in novel therapies for the treatment of GBM. We also seek to optimize the configuration of the thermo-gelling hydrogels within the resection cavity to maximize drug delivery to the surrounding brain.

Keywords: Paclitaxel, Glioblastoma multiforme, controlled-release, thermo-gelling polymers

INTRODUCTION:

Approximately each year in the United States there are 22,500 new diagnoses of malignant primary brain cancers. [1] Gliomas, the most common form of primary brain cancers in adults, account for nearly 51% of all central nervous system (CNS) tumors. [2] The most aggressive form of glioma and primary brain cancer is glioblastoma multiforme (GBM), which has a worldwide annual incidence of 74,000 cases and a median overall survival (OS) of approximately 9 months. [2-5] Treatments for primary malignant gliomas range from surgical resection [6, 7] to external beam radiation and chemotherapy. [8, 9]

A common practice in cancer treatment is the use of systemic therapy. These therapies have many inherent drawbacks, such as harmful side effects (e.g. vomiting, hair-loss, and uncontrolled weight loss). However, the biggest drawback of systemic therapy is decreased concentrations of drug reaching the target area due to dilution effects as the drug passes through the body. Another important limitation in systemic cancer treatment for brain malignancies is the blood-brain barrier (BBB). The BBB is a highly impermeable barrier due to tight-junction formation of endothelial cells. The BBB formed by cerebral endothelial cells is unique in the degree of "tightness" achieved, which inhibits efficient drug transport from the circulating blood to the cerebrospinal fluid (CFS). [10-12] Most systemically administered therapies do not adequately penetrate to the brain tumor tissue as a result of this biological barrier. Therefore, employing localized therapies that are directly placed within the resection cavity allow for a far greater drug selection and potential effectiveness.

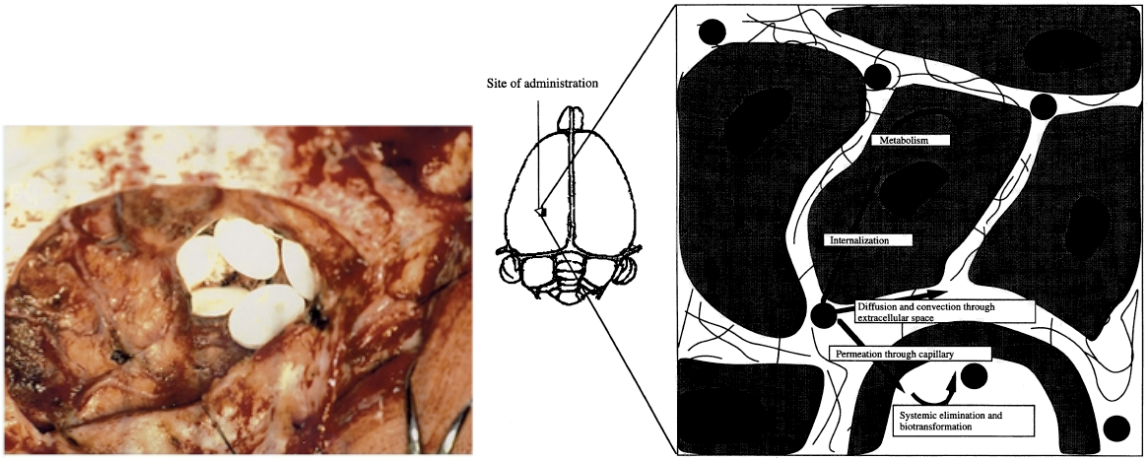

Figure 1: A) Implantation of Gliadel® wafers into a resection cavity. [13] B) Mechanism of drug metabolism and elimination from the brain. [14]

Upon surgical resection, local chemotherapy may be administered to the resection cavity via the use of carmustine (BCNU, 1,3-bis[2-chloroethyl]-1-nitrosourea) loaded wafers (Gliadel® wafers by MGI Pharma). The wafers are 14 mm x 1 mm biodegradable p(CCP:SA) (20:80 poly[bis] (p-carboxyphenoxy) propane/sebacic acid) discs loaded with 3.85% (7.7 mg) BCNU, where drug is released through a controlled release mechanism from the biodegradable matrix. [15] After surgical resection up to 8 wafers are implanted into the resection cavity where they will be subsequently subjected to natural brain fluids, which penetrate and degrade the porous matrix, allowing BCNU to diffuse into the surrounding brain parenchyma. (Figure 1)

However, one significant limitation of this modality is the instability of BCNU in aqueous media; the half-life ($t_{1/2}$) of BCNU is approximately 110 minutes. [16] In addition to the drug's instability, carmustine has high capillary permeability thus causing rapid elimination from the brain tissue, and thus affecting the efficacy of the treatment. [16] The largest problem, augmented by the limitations of BCNU, is GBM recurrences appear in an area up to two centimeters from the initial excision cavity, while penetration

of the drug is limited to a few millimeters from the polymer-tissue interface. [16-18] Due to these inherent limitations alternative approaches for localized chemotherapy are needed that result in sustained and effective drug concentrations at farther distances from the resection cavity.

One such modality that is being actively explored is the use of polymeric carriers for the controlled delivery of paclitaxel. The polymeric carrier method allows for prolonged, sustained continuous and predictable local release of drug, while simultaneously limiting systemic exposure. [15] As described in Fung and Saltzman [19], the classes of polymers, range from proteins to polyacrylates and silicone elastomers and are characterized by whether they are permanent implants or biodegradable ones, and by their biocompatibility.

Paclitaxel, an anti-microtubule, anti-neoplastic agent isolated in 1963 from the pacific yew *Taxus brevifolia*, functions by promoting assembly and stabilization of microtubules, thereby inhibiting cell proliferation. [20, 21] It has been shown that the degradation rate is much slower than that of carmustine and effective in both *in vitro* and *in vivo* against glioma cells. [12, 21-23] However, the half-life depends upon the duration of infusions. [20] In addition, the hydrophobic nature reduces the capillary permeation in brain tissue. [16]

A promising new type of polymeric carrier for the treatment of GBM is a novel set of thermo-gelling block-copolymers, poly(DL-lactide-co-glycolide-b–ethylene glycol-b-DL-lactide-co-glycolide) (PLGA-PEG-PLGA) capable of conforming to the shape of the resection cavity and providing the same or better sustained release of paclitaxel, than it's predecessor, PEG-PLGA-PEG tri-block co-polymers. [24-28] When these polymers

are below the critical gelation temperature (CGT), they can be easily loaded with hydrophobic drugs in solution and above the CGT, the polymers form drug-releasing hydrogels. Below the CGT, micelle formation works as a surfactant, increasing the solubility of hydrophobic drugs maximally 2000-fold in aqueous solutions of these polymers. [29]

Many agents that show great promise *in vitro* and in animal models often have little to no impact on the disease clinically. Animal models are necessary, but have significant disadvantages when attempting to correlate those findings with the human response. In particular, the size of the rat brain is small enough to allow efficient diffusive delivery and therefore, results that are often found in rat models cannot be correlated with the human response. One way to predict the effectiveness of a drug delivery system is to use computational modeling based on the characterization of the drug transport properties. However, experimental determination of the polymer must be carried out to obtain the necessary parameters for the modeling systems.

We seek to show that thermo-gelling polymeric carriers of paclitaxel can be a novel and effective therapy in the treatment of GBM on the basis that drug diffusion is occurring at a sufficient rate to provide therapeutic concentrations to the resection cavity before degradation of the hydrogel occurs. Analogs, in the form of dyes or molecular markers are used to mimic the properties of paclitaxel and carmustine. Solubility and diffusivity of the analogs need to be characterized and optimized. This work should further the process of developing alternative paclitaxel loaded hydrogel treatment strategies for the treatment of primary and relapsed/refractory GBM.

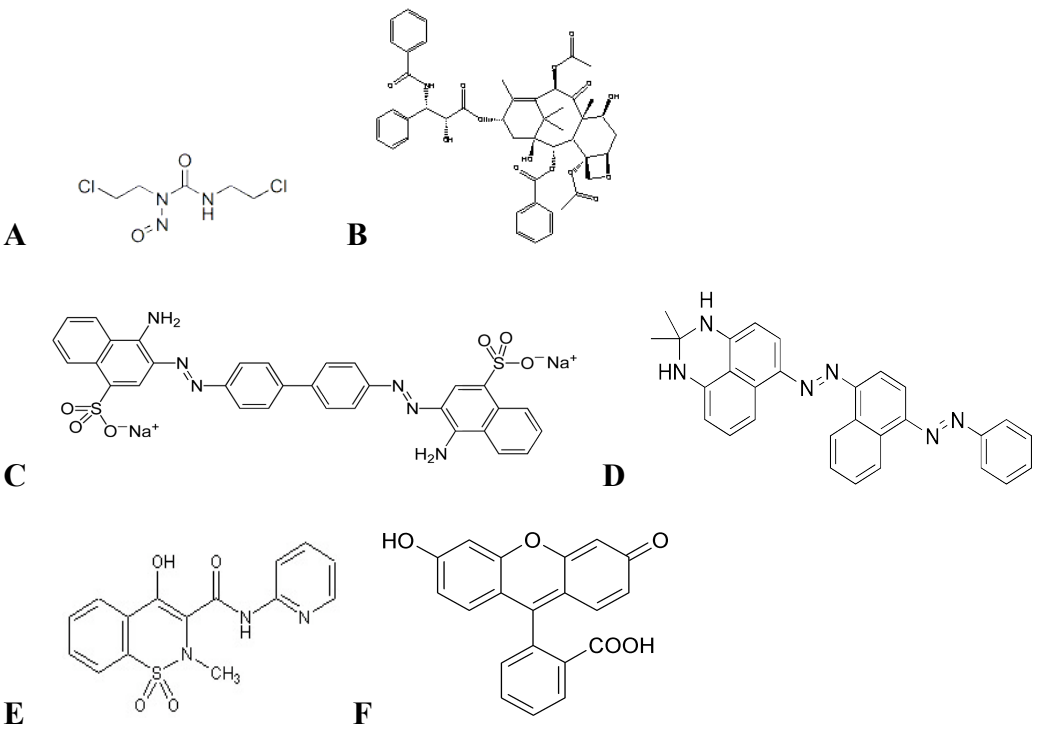

Figure 2: Chemical Structures of drugs and analogs. A) Carmustine B) Paclitaxel C) Congo Red D) Sudan Black B E) Piroxicam and F) Fluorescein.

MATERIALS AND METHODS

CREATING STOCK DYE SOLUTIONS AND CALIBRATION CURVES

Stock solutions of each dye were made by dissolving in DPBS to create 108 μM solution of fluorescein (Sigma, $C_{20}H_{12}O_5$; M_w = 332.32, E_{max} = 490 nm in 0.1 M Tris at pH 8.0); 517 μM solution of Congo Red (Sigma, $C_{32}H_{22}N_6Na_2O_6S_2$; M_w = 696.68; 40% dye content; E_{max} = ~500 nm; solubility: 0.03g/mL of H_2O); and 679 μM Sudan Black B (Sigma, $C_{29}H_{24}N_6$; M_w = 456.54; E_{max} = 598 – 605 nm; solubility: 0.1 mg/mL in H_2O). Due to the hydrophobic nature of Sudan Black B, 0.5% by volume of Tween 20 (1.25 mL) was added to the DPBS buffer solution. The addition of Tween 20 ensures a smoother calibration curve and the ability to obtain more data. The effect of Tween 20 on the solubility of Sudan Black B in solution is negligible. (Figure 2)

The concentration of the primary stock solution for each dye was calculated and subsequently diluted by a factor of 2 to obtain the concentrations to be used as the standards. The samples were then run on a spectrophotometer (BIO-RAD SmartSpec 3000^{TM}) for Fluorescein and Congo Red, and a 96-well plate spectrophotometer (Molecular Devices SoftMax® Pro Version 4.3 Software) for Sudan Black B and Piroxicam (Sigma, $C_{15}H_{13}N_3O_4S$; M_w = 331.37; E_{max} = 276 nm) to obtain the absorbance of each standard at E_{max}.

Dyes are also loaded into the hydrogels to create a calibration curve of dye in the hydrogel. From our library of polymers (Appendix A) AT-19 [PLGA-PEG-PLGA; 1,000-1,000-1,000 (3:1, DL-lactide/glycolide)] was chosen for Fluorescein and Congo Red and AT-21 [PLGA-PEG-PLGA; 1,142-1,000-1,142 (2.7:1, DL-lactide/glycolide)] was chosen for Congo Red, Sudan Black B and Piroxicam. Dye was loaded into the AT-19 matrix along with DPBS using the Equation (1):

$$\delta = \frac{\alpha - 0.23\alpha}{0.23} \tag{1}$$

where α is the grams of AT-19 and δ is the grams of DPBS + dye. Since AT-19 is soluble up to a 37 weight % (Figure 3a), solutions of AT-19 were created at 23 weight %. Equation (2) was then used to convert δ from Equation (1) to μL to determine the amount of DPBS + dye solution needed to create the 23 weight % hydrogel:

$$x = \left(\frac{\delta}{1.1}\right) \times 10^3 \tag{2}$$

where x is the μL of DPBS + dye, δ is the grams of DPBS + dye and 1.1 is the density of the polymer. To obtain the concentration of dye that would actually be in the hydrogel solution the standard dilution equation was used:

$$V_1 C_1 = V_2 C_2 \tag{3}$$

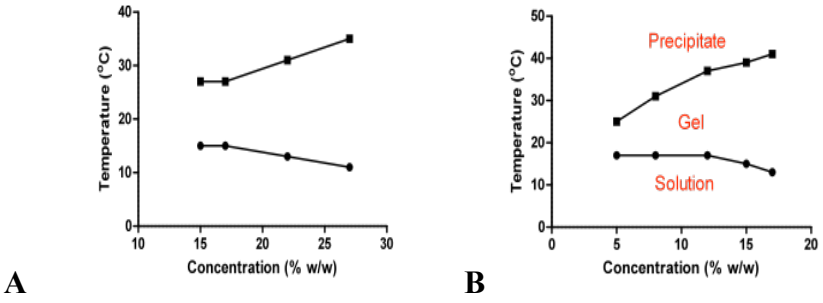

Figure 3: Thermo-gelling hydrogel matrix of poly(ethylene glycol-co-L-lactide-co-glycolide) as novel drug delivery system. A) Phase diagram of thermo-gelling polymer PLGA-PEG-PLGA; 1,000-1,000-1,000 (3:1, DL-lactide/glycolide) at different concentrations in aqueous solution. B) Phase diagram of thermo-gelling polymer PLGA-PEG-PLGA; 1,142-1,000-1,142 (2.7:1, DL-lactide/glycolide) at different concentrations in aqueous solution. Maximum solubility of PLGA-PEG-PLGA; 1,000-1,000-1,000 (3:1, DL-lactide/glycolide) is 37% and maximum solubility of PLGA-PEG-PLGA; 1,142-1,000-1,142 (2.7:1, DL-lactide/glycolide) is 17%.

---

where V_1 is the volume of DPBS + dye in mL, C_1 is the concentration of the DPBS + dye that will be need to be added to the polymer, V_2 is the volume of polymer and C_2 is the standard concentration to be chosen from the calibration curve of dye in buffer. Combining Equations (1), (2), and (3) C_1 can be determined by the following equation:

$$C_1 = \frac{\left[(\alpha + \delta)\left(\frac{1mL}{1g}\right)\right](\gamma)}{\left(\frac{\delta}{1.1}\right)} \tag{4}$$

where γ is the chosen concentration from the dye in buffer calibration curve.

Despite the polymers being synthesized following the same protocol, the physical properties of the polymers in the library differ slightly. AT-21 is soluble only up to 17 weight % (Figure 3b), therefore, the 0.23 term in Equation 1 was substituted with 0.17. Upon loading the dye solution in the polymer matrix, the solution was placed in a spinning rack at 4°C overnight for AT-19 and two days for AT-21 to allow homogenization of dye and buffer.

ENSURING HOMOGENOUS SOLUTION OF DYE IN HYDROGEL

After the allotted time mentioned above was reached, a 100μL sample was taken out in triplicate and measured in the respective spectrophotometer. If the absorbance readings were no greater than double, then it was assumed that the solution was homogenous.

BRAIN PHANTOMS

The brain phantoms were adapted from The Brain Phantom Project [30]: however, the phantoms only contained 0.6% agarose and de-ionized H_2O (dH_2O) obtained from the NanoPure water filtration system. Deviations from the original protocol were necessary because Tris, 0.5M EDTA and Boric Acid, all of which are used in the original protocol, affect the formation of the hydrogel placed within the resection cavity. To create a 0.6% agarose brain phantom: 7.8 grams of agarose is dissolved in 1300 mL of dH_2O by placing the solution in the autoclave on a "liquid cycle" (15-minute sterilization). The solution is allowed to cool for 30-45 minutes before pouring into the casting mold. To create the resection cavity with a constant volume, a fully inflated endotracheal (ET) tube is placed into the agarose and secured in place. The casting mold with ET tube is then placed in 4°C overnight. (Figure 4) A 0.6% agarose concentration strikingly resembles the human brain when considering certain critical physical characteristics such as the human brain's macroscopic characteristics (e.g. porosity, penetration values, drag forces). [31]

DYE RELEASE PROFILES

From hydrogel into buffer: In order to optimize and correlate the paclitaxel release profile within the brain with the dye analogs, diffusion coefficients must be determined. To

A 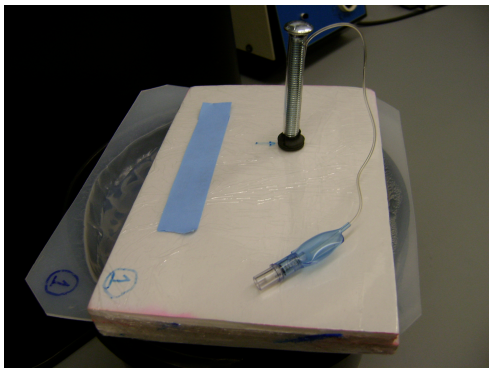

B 

Figure 4: Agarose Brain Phantom Model. A) Experimental set-up: Styrofoam holding inflated ET tube vertically to create the resection cavity within the 0.6% agarose brain phantom model. B) 0.6% agarose brain phantom model

---

achieve this goal, a constant concentration boundary condition was established. Piroxicam is dissolved into AT-21 polymer solutions at 2 mg/mL. After allowing homogenization, 600 µL of the polymer solution is loaded in duplicate into wells of a UV-transparent 24-well plate (BD Falcon™), which is placed at room temperature until the solution became a hydrogel. Two mL of DPBS + 0.5% Tween 20 is then pipetted over each gel and covered with a polyester adhesive film (VWR) to minimize evaporation. The entire set-up is then wrapped in parafilm and aluminum foil, which minimizes light exposure and placed at 37°C in a humid incubator with gentile agitation. At predetermined time-points, 100 µL samples of the supernatant are extracted and the absorbance read at E_{max} = 276 nm. Two mL of fresh DPBS + 0.5% Tween 20 is subsequently added. The data is then plotted and fitted to the equation:

$$\frac{M_t}{M_\infty} = 2\sqrt{\frac{\Delta t}{\pi L^2}} \tag{5}$$

The cumulative mass % is plotted over the square root of time ($\sqrt{t}$), to obtain a linear plot where the slope, $\frac{2}{L}\sqrt{\frac{D}{\pi}}$ is used to solve for the diffusion coefficient, D. [32]

From hydrogel into brain phantom: After brain phantoms were prepared as outlined above, the resection cavity was filled 30% (8.3 mL) with hydrogel and allowed to sit at room temperature. To minimize "sweating" of the agarose, the phantoms were covered with clear plastic wrap. Because of the photosensitivity of Piroxicam, the brain phantoms were also kept in the dark for the duration of the experiment. At predetermined time-points (t =0, 3 and 7 days post injection) the absorption of the dye from the hydrogel was measured and plotted to determine the release profile.

COMPUTATIONAL MODELING

The transport model consisted of fluid, mass and drug transport created by Dr. Alexis Torres in our lab. Fluid transport in the brain is assumed to behave as a homogeneous porous media where the fluid has achieved steady state. It is also assumed that the surgery resulted in gross-total resection of the tumor and only scattered malignant cells remain in proximity to the cavity. Dimensions were taken from a magnetic resonance image (MRI) of a patient and used to construct an anatomically correct model. A two-dimensional model was used to reduce the computational time. A very important distinction that was not considered in the model was the difference between grey and white matter.

The transport of fluid was assumed to have the same rheological properties as water at 37°C and can be described by combining the equation for mass conservation and the momentum equation for fluid flow. [32-34] Fluid removal via the lymphatic system (F_l) is assumed to be negligible due to the lack of a well-defined lymphatic system in the brain.

Onset of edema after surgical resection is characterized by an increase in fluid in the extracellular space (ECS), resulting in an increase in hydraulic conductivity of the blood capillaries and serum leakage from the cerebral blood vessels. The variation of hydraulic conductivity with time in this model was taken from previous reports. [32, 33] It was also assumed that the surrounding hydraulic conductivity (within 3 mm) is uniformly affected by edema. The current model uses the following equation [32]:

$$L_p = L_{p0}(1 + ae^{-bt}) \tag{6}$$

where t is time in seconds and a and b are 9×10^{-5} and 1.94×10^{-5} s^{-1} respectively. As a result of employing this equation, tumor hydraulic conductivity increases ten-fold from normal tissue and is 94% resolved at $t = 3$ days.

The tissue immediately surrounding the polymer implant consists of three distinct phases: interstitial/extracellular space (ECS), intracellular space (ICS), and the cellular membrane (M); and drug is always present in either a free or bound form. Free drug is present throughout all three phases, and the molar concentration of drug per total tissue volume, C, is expressed as [14, 16, 32]:

$$C = \alpha C_{ECS} - \beta C_{ICS} + (1 - \alpha - \beta) C_M \tag{7}$$

where C is the average free drug concentration, C_{ECS}, C_{ICS}, and C_M are the free drug concentrations in the extracellular, intracellular, and cellular membrane spaces respectively, α and β are the volume fractions of the extracellular and cellular spaces respectively. The following partial differential equation describes the local concentration of drug molecules in brain tissue, assuming isotropism [14, 16, 32]:

$$\left(\frac{\partial C}{\partial t}\right) = \alpha D_{ECS}\nabla^2 C_{ECS} - \nabla\cdot(VC_{ECS}) - \alpha(k_{bbb} + k_e)C_{ECS} - \beta k_e C_{ICS} - (1 - \alpha - \beta)k_M C_M - \frac{\partial B}{\partial t} \tag{8}$$

where t is the time after implantation, D_{ECS} is the diffusion coefficient of the drug in the ECS, V is the fluid velocity field vector (derived by solving Darcy's equation), and k_{bbb} and k_e are first-order elimination constants of capillary permeation and enzymatic/non-enzymatic elimination respectively. To simplify, the following assumptions can be made: the drug is not bound or eliminated in the membrane phase, the concentration of bound drug is directly proportional to the concentration of free drug in the ECS and ICS (i.e., $K_{ECS} = B_{ECS}/C_{ECS}$ and $K_{ICS} = B_{ICS}/C_{ICS}$), drug is eliminated by a first-order process and free drug is present in all three phases and in local equilibrium. Based on these assumptions, Equation (7) and (8) can be combined to give the general expression in terms of C_{ECS} [32]:

$$\frac{\partial C_{ECS}}{\partial t} = \left(\frac{\alpha}{\alpha^*}\right) D_{ECS} \nabla^2 C_{ECS} - V.\nabla C_{ECS} - \left(\frac{\alpha (k_{bbb} + k_e) + \beta k_e P_{I/E} + F_V}{\alpha^*}\right) C_{ECS} \tag{9}$$

where α^* is a constant that accounts for the effects in solute transport by local binding and cell membrane partitioning. [32]

In the cavity, 100% of the drug is available for transport in the interstitial phase, and binding and partitioning is assumed to be negligible, and diffusion and convection take place freely. As a result, drug transport in the interstitial medium is expressed dependent of time by solving Darcy's equation of fluid flow as illustrated [32]:

$$\frac{\partial C_{ECS}}{\partial t} = D_{ECS} \nabla^2 C_{ECS} - V \nabla C_{ECS} - k_C C_{ECS} \tag{10}$$

where k_c is the first-order degradation constant in the cavity. It was assumed that flow reaches equilibrium faster than drug diffusion. COMSOL Multiphysics 3.5a was used to simulate the fluid, mass, and drug transport.

RESULTS

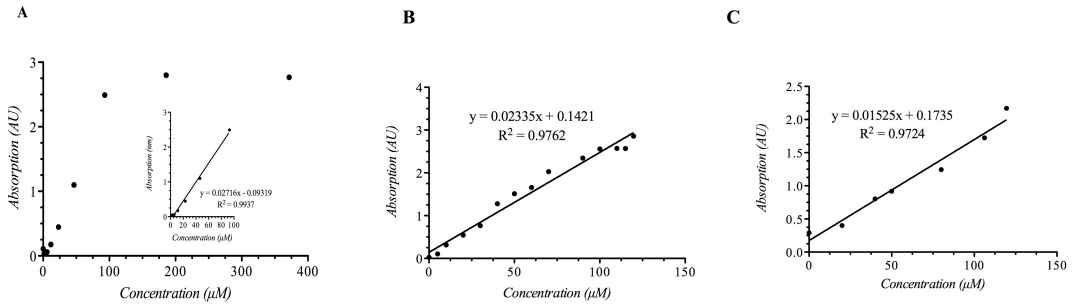

Figure 5: Calibration Curve of Congo Red. A) Congo Red in DPBS buffer solution, B) Congo Red in PLGA-PEG-PLGA; 1,000-1,000-1,000 (3:1, DL-lactide/glycolide), C) Congo Red in PLGA-PEG-PLGA; 1,142-1,000-1,142 (2.7:1, DL-lactide/glycolide). All readings were done at E_{max} = 479 nm

---

CALIBRATION CURVES

Maximum concentrations were obtained by choosing the highest value still within the linear region of the calibration curve. This value indicates the maximum concentration that can be read accurately by the spectrophotometer. A maximum concentration of 39 μM was found for Fluorescein at an E_{max} = 490 nm in DPBS. (Data not shown) The maximum concentration of Congo Red was found to be 120 μM, at an E_{max} = 479 nm in DPBS. (Figure 5A)

The maximum concentration of Sudan Black B was found to be 679 μM at an E_{max} = 575 nm in DPBS + 0.5% Tween 20. (Figure 6A) This concentration was not the maximum concentration in the linear region; however, this concentration was chosen because a saturated solution was achieved 679 μM, above this concentration Sudan Black B would no longer dissolve in solution. A maximum concentration of 1.8 mM was previously found for Piroxicam at an E_{max} = 276 nm. (Figure 7A)

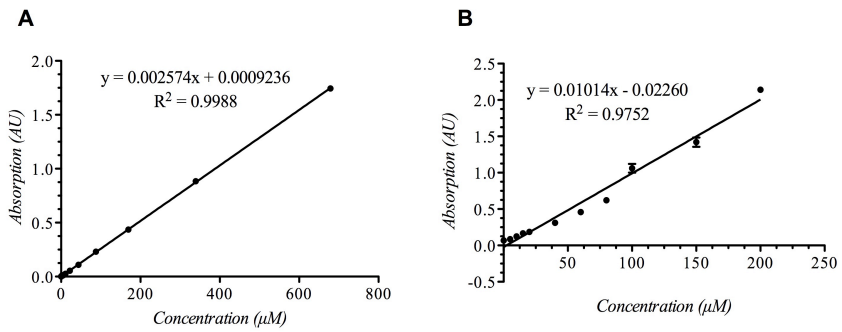

Figure 6: Calibration curve of Sudan Black B: A) Sudan Black B DPBS solution plus 0.5% by volume Tween 20 B) Sudan Black B in PLGA-PEG-PLGA; 1,142-1,000-1,142 (2.7:1, DL-lactide/glycolide). All readings were done at E_{max} = 595 nm.

The calibration curve of Fluorescein loaded in AT-19 was unable to be determined due to the polymer inducing a quenching effect on the dye, therefore the measured absorbance was lower than what would be expected for the specific standard and, as a result, could not be correlated back to the standard concentration. (Data not shown). There were no quenching effects seen for Congo Red in AT-19 or AT-21, Sudan Black B or Piroxicam. (Figures 5B and 5C, 6B and 7B respectively)

RELEASE PROFILES

Congo Red and Sudan Black B were continuously released from AT-21 while immersed in DPBS + 0.5% by volume Tween 20. The release of Congo Red was done both at room temperature and at physiological temperature (37°C). (Appendix B) Since Sudan Black B is extremely hydrophobic, the release was only done at physiological temperature only.

The diffusion coefficients for Congo Red and Sudan Black B however, could not be calculated accurately due to significant evaporation (> 20%). The calculated diffusion coefficient, $D_{Congo\ Red\ RT}$ for Congo Red at room temperature was determined to be 1.8 mm^2/hr and 2.1 mm^2/hr for $D_{Congo\ Red\ 37°C}$. (Since novel hydrogels are being used the

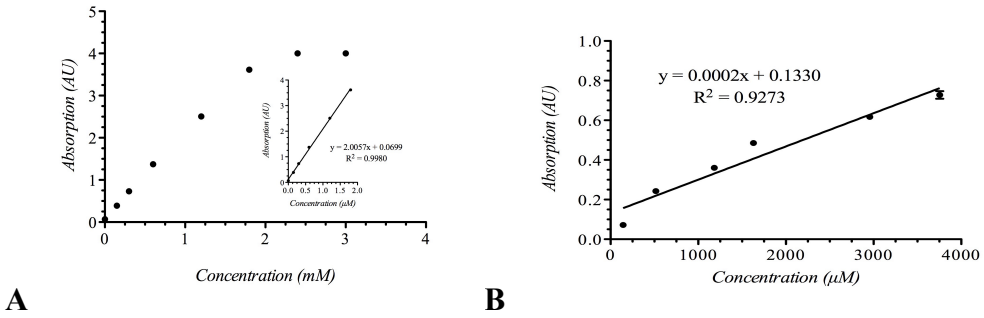

Figure 7: Calibration curve of Piroxicam: A) Piroxicam in DPBS plus 0.5% by volume Tween 20, B) Piroxicam in PLGA-PEG-PLGA; 1,142-1,000-1,142 (2.7:1, DL-lactide/glycolide). All readings were done at; E_{max} = 276 nm.

---

diffusion coefficient of Congo Red out of this medium is unknown, and as a result, no comparison can be made.) In addition to evaporation, the supernatant contained only DPBS, which may explain the initial 1.93% release of Sudan Black B, over the first 5 hours followed by a plateau. (Data not shown). As previously mentioned, the addition of 0.5% by volume of Tween 20 could have aided in gathering more data points for Sudan Black B, thus allowing the determination of the diffusion coefficient. Piroxicam was also continuously released from AT-21 immersed in DPBS + 0.5% Tween 20 at physiological temperature. (Figure 8A) The diffusion coefficient $D_{Piroxicam}$ was calculated to be 24.56 mm^2/hr. The diffusion coefficient of Congo Red at physiological temperature is slower than that of carmustine, 5.148 mm^2/hr and paclitaxel, 3.24 mm^2/hr, while Piroxicam is much faster, making both dyes unsuitable for analogs. The rate of release of Piroxicam (Figure 8B) dropped exponentially over time and was approximated as follows [16]:

$$\left[\frac{dM_t}{dt}\right]_{buffer} = \frac{M_n - M_{n-1}}{t_n - t_{n-1}} \qquad (11)$$

where t_n is the time elapsed until collection of the n^{th} sample, and M_n is the mass of dye released into DPBS + 0.5% Tween 20 between fluid exchanges t_n and t_{n-1}. An interesting

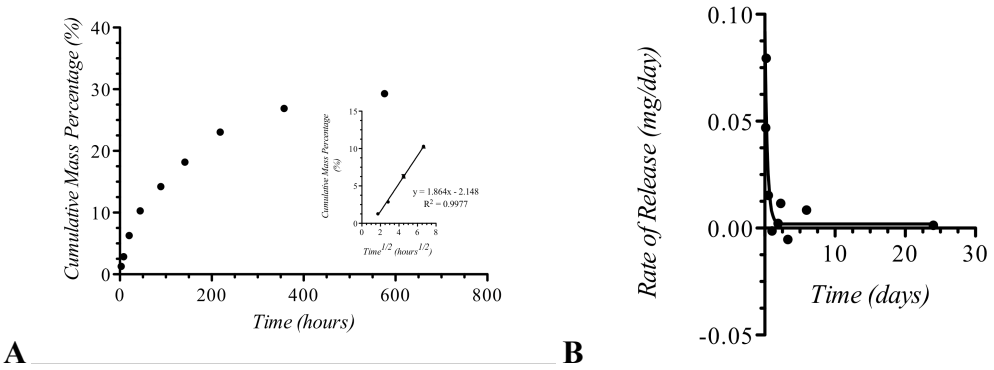

Figure 8: Release Profile and Rate of Release of Piroxicam out of poly(ethylene glycol-co-L-lactide-co-glycolide) polymer PLGA-PEG-PLGA; 1,142-1,000-1,142 (2.7:1, DL-lactide/glycolide). A) Plot of cumulative mass % at E_{max} = 276 nm released over time. Insert is the linear region vs. square root of time. $D_{piroxicam}$ = 24.56 mm^2/hr B) Rate of release of Piroxicam over time.

phenomenon was observed; it appears that the hydrogel interacts with the dye, only allowing an initial release of dye, which can be considered to be in an unbound form with respect to the hydrogel. (Seen as the plateau on the release profiles.) One hundred percent cumulative release was not achieved for any of the release profiles. 21.5% of Congo Red was seen free to diffuse out of the matrix into the supernatant, while the remainder was bound. As previously mentioned, 1.93% of Sudan Black B was free to diffuse and 29.3% for Piroxicam. It can be assumed, then, that the difference is the percentage of the binding interactions between the polymer and dye. However, this inference can only be qualitative because there is no standard to quantitatively compare too.

BRAIN PHANTOMS

Two brain phantoms were injected with AT-19/Congo Red hydrogel solutions, and the percentage of dye remaining in the matrix after *t* = 3 and 7 days were found to exponentially decrease. (Figure 9a) A similar result was observed with AT-21/Piroxicam hydrogel solutions when samples were taken at *t* = 1,3 and 7 days. (Figure 9b) However,

at t = 7 days the percentage remaining was 74.4%. (Data not shown). This problem arises because each time-point requires a separate brain phantom, therefore, release is not continuous from the same polymer over the entire experiment despite the solutions being nearly identical in each phantom. The result seen for t = 7 days may have been from a combination of binding interactions between the polymer matrix and the volume of the resection cavity decreasing. A decrease in the resection cavity volume results when the inflated ET tube is placed in a hot media causing the balloon to deflate. The shape of the curve indicates that the hydrogel is establishing a typical first-order controlled release mechanism and is consistent with a diffusion-controlled release mechanism. If these experiments were allowed to run until all of the dye was released from the matrix into the surrounding agarose, the release mechanism would likely have been faster than a purely diffusion-controlled mechanism, which would likely be the result of combined diffusion and polymer degradation mechanisms. [29] Since convection results in higher fluid velocities than diffusion, the presence of a minimal amount of convection could make a substantial difference.

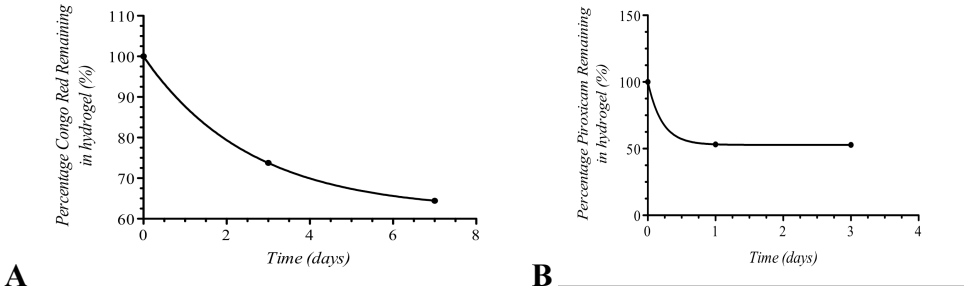

Figure 9: Time-lapse diffusion of Congo Red out of thermo-gelling hydrogel from resection cavity of brain phantom model. A) 33% of the resection cavity in the brain phantom model was filled with PLGA-PEG-PLGA hydrogel loaded with Congo Red and absorbance was read at 3 and 7 days post-injection. B) Repeated experiment instead with Piroxicam readings taken at 1 and 3 days post-injection. (At Day 7: 74.40% still remained in the cavity).

It was also observed that the hydrogel was not allowed to completely solidify in the resection cavity of the brain phantom. This may have been the result of increasing water content due to "sweating" when the polymer was loaded into the phantom and allowed to solidify in the resection cavity.

TRANSPORT MODEL

Keeping all parameters consistent with our lab's previous study, the transport model was run with different arrangements of hydrogel within the resection cavity. [32]

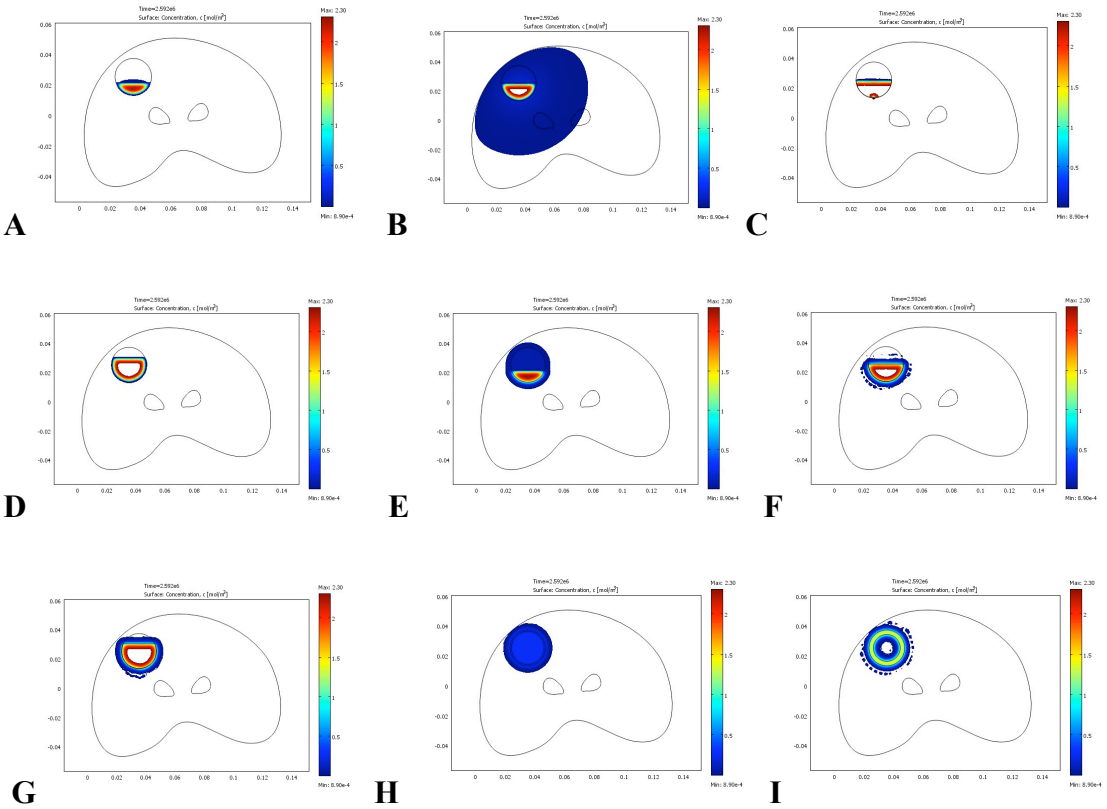

Figure 10: Computer Simulation of Drug Release into Brain when filling the resection cavity: A) 30% carmustine-loaded hydrogel, B) 50% carmustine-loaded hydrogel, C) Corrected 50% carmustine-loaded hydrogel D) 66% carmustine-loaded hydrogel, E) 30% paclitaxel-loaded hydrogel, F) 50% paclitaxel-loaded hydrogel, G) 66% paclitaxel-loaded hydrogel. H) 1.0 mm lining of paclitaxel-loaded hydrogel, I) 3.0 mm lining of paclitaxel-loaded hydrogel. Displayed concentrations have cut-off values to account for differences in minimum therapeutic concentrations of carmustine (0.0150 mol/m^3) and paclitaxel (8.90×10^{-4} mol/m^3)

The model hydrogel was loaded with either paclitaxel or carmustine and run for a simulated 30 days (the maximum time where predictable release can be expected due to the onset of polymer degradation).

The surface concentration was kept constant at 2.34 mol/m^3 for comparative analysis; each simulation was repeated for carmustine and paclitaxel loaded in hydrogel and compared with the release from Gliadel® wafers. The two-dimensional resection cavity is represented by a circle with a diameter of 2.0 cm corresponding with a spherical volume of 4.19 cm^3 in three dimensions.

The cavity was filled with 30%, 50% or 60% with a thermo-gelling polymer matrix. (Figure 10a-f) Release of carmustine when the hydrogel filled 30% and 60% of the resection cavity showed no penetration into the surrounding tissue; and only a small amount of penetration into the resection cavity when the resection cavity was filled 30%. (Figure 10a, c) However, filling 50% of the cavity with carmustine-loaded hydrogel yielded significant penetration of the minimum therapeutic concentrations into the surrounding brain. (Figure 10b) Upon review, several of the boundary parameters in the model were incorrect, and when corrected, the model yielded similar results to filling the resection cavity 30% and 66%. (Figure 10i) Filling the resection cavity with any of the three percentages was less effective than Gliadel® wafers at 36 hours post implantation, therefore, not an effective arrangement. (Figure 11a) Compared with paclitaxel-loaded hydrogels, increased penetration of drug was seen in all three arrangements (30%, 50%, and 60%), however, penetration of paclitaxel was limited to only about 4.0 – 5.0 mm. (Figure 10d-f) This is slightly better than release from the Gliadel® wafers at 30 days post implantation. (Figure 11b)

Further simulations were run with the thermo-gelling polymer matrix lining the resection cavity with a 1.0 mm or a 3.0 mm thickness. (Figure 10g and h) When lining the resection cavity with carmustine-loaded hydrogels, neither with 1.0 mm nor 3.0 mm layers, at the same surface concentration, showed any result. The surface concentration needed to be at least three orders of magnitude higher (a concentration that would certainly be above the maximum tolerated dose (MTD) for carmustine) to provide results. This most likely results from the concentration being smaller than the elimination constant of carmustine in the cavity, blood capillaries, and from enzymatic/non-enzymatic reactions, all of which are incorporated into the transport model. Since the concentration is smaller than the elimination constant, carmustine is eliminated from the system at a rate that does not allow for penetration and therapeutic benefits.

Lining with paclitaxel-loaded hydrogel at both thicknesses showed penetration into the surrounding brain, only at a distance of a few millimeters. (Figure 10g,h)

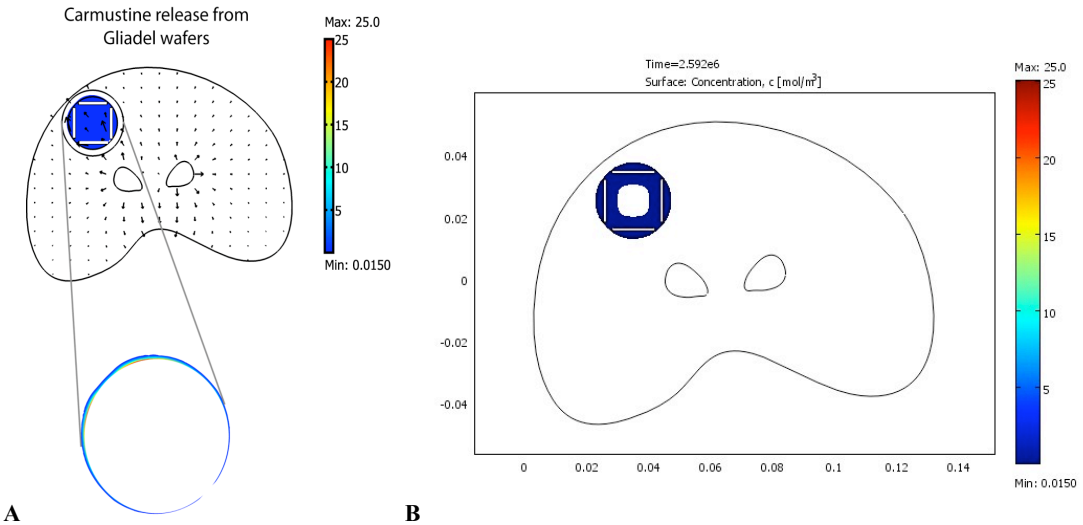

Figure 11: Carmustine release from Gliadel® wafers in transport model: Drug penetration profile of carmustine (a) 36 hours post implantation and (b) 30 days post implantation. Displayed concentrations have cut-off values to account for differences in minimum therapeutic concentrations of carmustine (0.0150 mol/m^3)

Employing a 1.0 mm layer of paclitaxel-loaded hydrogel around the resection cavity provided the greatest penetration to the resection cavity and surrounding brain parenchyma. This thickness could be obtained by coating the cavity with the gel or immobilizing it on a scaffold (e.g., Surgicel^{TM}). Lining the resection cavity proves to be the most optimal arrangement of the hydrogel within the resection cavity. Despite all paclitaxel loaded hydrogel configurations exhibiting approximately the same amount of penetration, lining the cavity would allow more drug to diffuse out rather than being trapped in the polymer matrix, a result of the surface area to volume ratio, exhibited when comparing Figure 10f and 10h. A 1.0 mm lining or slightly greater (< 3.0 mm) would provide the best penetration, which is better then the standard Gliadel® wafers.

DISCUSSION

Discovering effective novel delivery mechanisms of anticancer agents to treat malignant gliomas is a challenging task. Currently, there exists a wide range of treatments for primary and relapsed/recurrent malignant gliomas. Local delivery of chemotherapeutic agents is a promising treatment modality. However, many factors prevent drug diffusion to the tumor in both local and systemic treatment, the greatest being the BBB.

The BBB is a combination of a basement membrane and an endothelial monolayer that allows only lipophilic molecules smaller than ~500 Da to pass through. [35] For drugs to penetrate the BBB, the drug must be lipophilic (e.g., paclitaxel or BCNU), targeted towards a membrane transporter, and/or the BBB needs to be osmotically disrupted (e.g., super-selective intra-arterial cerebral infusion after mannitol disruption) or its vasculature permeabilized. [35, 36] However, even when treatments

eventually pass the BBB, their concentrations are usually too low to be effective. BCNU or the more lipophilic paclitaxel will readily traverse the BBB, but only a limited number of tumor cells will be killed while leaving normal cells alone, and it is not possible to conjugate targeting moieties while maintaining the necessary size for crossing. [35] As a result, local delivery methods are essential.

BCNU has been the standard of care for localized delivery, but despite being well tolerated from a toxicity perspective, it only produces moderate results in prolonging OS due to a sharp decrease in concentration as the distance from the implant site increases. [35] As a result, the flux of drug from the implant to the surrounding brain parenchyma is mostly a function of the concentration at the implant site. This limitation, in addition to the short half-life of BCNU, and high capillary permeability, leads to the search of new, more effective lipophilic drugs and methods such as the novel thermo-gelling hydrogels used in this study.

The much more hydrophobic paclitaxel may be a more effective drug of choice because of the slower degradation rate and decreased capillary permeation in brain tissue. [16] Though the diffusivity of paclitaxel is similar to carmustine, it is subjected to much less elimination by transcapillary exchange mainly due to its larger molecular size. [33] It is also a known radio-sensitizer and could be combined with radiation therapy to increase the effective targeting and killing of cancerous cells, thus making it a good candidate for localized delivery. [32, 37]

The employment of thermo-gelling polymers used in this study allows for a greater choice of therapeutic agents to be delivered for prolonged, sustained, continuous, and predictable concentrations and time periods. However, as shown filling the 30%,

50% or 60% of the resection cavity with the hydrogel, which subsequently conforms to the shape of the cavity, is not optimal for delivering effective concentrations of hydrophobic drugs to the brain parenchyma. When the hydrogel takes this arrangement within the resection cavity, the volume to surface area ratio is dramatically decreased, therefore, inhibiting a majority of the drug from diffusing out. This poses a potential risk when the polymer matrix starts to degrade, allowing for a sudden uncontrolled burst of drug into the surrounding brain. A sudden burst can lead to an adverse effect if the concentration is at or above the maximum tolerated dose for that particular drug.

This same phenomenon of reduced volume to surface area ratio is seen with the Gliadel® wafers. After trauma, the immediate physiological immune response is for the brain to swell. When this occurs in the brain after surgery, the resection cavity decreases in volume and the wafers that once lined the cavity will become stacked and, as a result, dramatically decrease the volume to surface area ratio, subsequently trapping a majority of carmustine and decreasing the efficacy of release. This phenomenon may help to partially explain the observed release profile curves; the thickness of the hydrogel may act similarly to the stacked wafers and trap the majority of the dye in the polymer matrix. It is possible that a layer less than 3 mm would yield a higher cumulative release. Additionally, binding interactions between the polymer matrix and the dye/drug may also help to explain why significantly less than 100% cumulative mass release was observed.

The synthesis of novel block co-polymers has led to the creation of a wide variety of stimuli-sensitive hydrogels, including thermo-sensitive, pH sensitive, and combined pH- and thermo-sensitive co-polymers. In addition, to various stimuli-sensitive hydrogels, the actual composition of hydrogels can also vary, such as poly(n-substituted

acrylamide)-based, poly(vinyl ether)-based, poly(ethylene oxide)-*b*-poly(propylene oxide)-*b*-poly(ethylene oxide) triblock polymers, also known as (Pluronic ®) or Poloxamer ®, or PEG and PLGA di- and tri-block co-polymers. [38] Depending on the function wanted and the location of implantation, different compositions are required. One of the original tri-block co-polymers was the PEG-PLGA-PEG tri-block; however, despite showing significant efficacy and a decrease in systemic adverse effects in Sprague-Dawley (SD) rats, newer generations of PLGA-PEG-PLGA tri-blocks were created. [38]

Choosing to synthesize novel thermo-gelling PLGA-PEG-PLGA hydrogels was fairly simple. Firstly, when treating in the brain, the pH does not and should not fluctuate; therefore, employing pH-sensitive hydrogels would not make sense (and could lead to adverse or even lethal effects if the pH of the brain were to fluctuate enough to activate the hydrogel sol-gel-sol phase transition). PLGA-PEG-PLGA tri-block co-polymers have already previously been shown to be efficacious in preliminary animal model studies, as well as clinical trials, and PLGA-PEG-PLGA polymers for therapy are already commercially available as ReGel® and OncoGel® (ReGel/paclitaxel). [23, 38]

Also, the synthesis of PLGA-PEG-PLGA has proven to be simpler than that of PEG-PLGA-PEG. The coupling procedure used to synthesize PEG-PLGA-PEG, hexamethylene diisocyante (HMDI), can be avoided. Another key difference between the two that makes PLGA-PEG-PLGA more desirable for the local treatment of gliomas, is PLGA-PEG-PLGA exhibited a reversible sol-gel-sol transitions with increasing temperature, along with other differences described in He et al. [38]

Brain phantoms are useful representations of the *in vivo* brain for testing diffusivity, novel treatments such as our thermo-gelling polymeric carriers, convection enhanced delivery (CED), and many more. The macroscopic characteristics of 0.6% agarose gel replicate that of the brain for surgical insertion of probes and are ideal for testing infusion studies. [31] However, major properties of the *in vivo* brain are ignored, such as differentiating between grey and white matter. The model is largely homogenous and isotropic, while brain tissue is quite inhomogeneous and highly anisotropic, especially in the white matter. Therefore, the flow pattern of the model would likely not replicate the natural complex flow pattern of the *in vivo* brain. [31] Secondly, the model is inert and unperfused, while brain tissue is quite perfused, making this model not useful for evaluating the uptake or clearance of agents in the brain. [31]

Many of the same properties are also ignored in our computational model. In order to provide a more realistic simulation in both the brain phantom and the computer model, these properties need to be considered. Computational modeling of drug transport to the brain showed only slight penetration, on the order of millimeters, into the brain. As previously mentioned, GBM tumors usually recur on the order of centimeters away from the initial resection site, therefore, drug penetration must reach these outlying malignant cells that persist in the tissue after resection. [16-18] Newer drugs that are angiogenesis inhibitors or immunomodulators, [15] such as bevacizumab, erlotinib, or temozolamide may provide better penetration; however, this still must be explored. Concurrent or combined treatment with other modalities such as stereotactic radiosurgery or cytokine immunotherapy [15] may also prove beneficial. It has been shown that concurrent

chemotherapy and radiosurgery have been able to prolong progression free survival (PFS) and OS slightly. [27, 36, 39, 40]

FUTURE STUDIES

Characterization and finding suitable dye analogs to paclitaxel or carmustine are needed. These analogs must have similar critical physical properties such as molecular weight and diffusivity. The release profile of Congo Red should be repeated, with minimizing evaporation following the procedure used for determining the Piroxicam release profile, considering the similarity to both paclitaxel and carmustine. In addition, the binding interaction must be characterized, and once this is accomplished, synthesize new tri-block thermo-gelling hydrogels that have protective groups to decrease the binding interactions. This may help achieve a greater sustained and controlled release of drug before the combined degradation/diffusion process begins. Additionally, the arrangement of the hydrogels still needs to be optimized to find penetration results comparable or better than the Gliadel® wafers. It is possible that completely new hydrogels need to be created to solve both of these problems. Furthermore, more realistic computer and brain phantom models should be constructed to account for the anisotropic and inhomogeneous properties of the *in vivo* brain as well as to differentiate between grey and white matter.

CONCLUSION

Thermo-gelling hydrogels are potentially novel alternative drug delivery systems for the localized treatment of GBM. In this study, the hydrogels used showed a controlled, but not sustained first-order release mechanism. Release was seen only to cumulative mass percentage of approximately 30%, which would provide few therapeutic

benefits for the patient. Release is inhibited by strong binding interactions between the dye and polymer matrix, therefore, further study is necessary to determine if this binding interaction can be avoided so higher release can be achieved. Fluorescein, Congo Red, Sudan Black B and Piroxicam are not suitable analogs for *in vitro* experiments of paclitaxel or carmustine. The diffusion coefficient of Piroxicam (24.6 mm^2/hr) was much faster than that of carmustine and paclitaxel, 5.148 mm^2/hr and 3.24 mm^2/hr respectively, while the diffusion coefficient of Congo Red at physiological temperature (2.1 mm^2/hr) was similar despite substantial evaporation. Computational modeling showed that lining the resection cavity with a 1.0 mm thick polymer matrix may provide the best therapeutic penetration; however, further study is required to optimize the therapeutic concentrations penetrating into surrounding brain parenchyma.

ACKNOWLEDGEMENT

Much of this project would not have been successful without the assistance of others. I would especially like to thank Dr. Alexis Torres and Charles Zhu for all of their invaluable help in troubleshooting and explaining the basic theory behind the project, fundamental biomedical and chemical engineering, and computational modeling. I would also like to thank Dr. Michael L Shuler for allowing me to complete my thesis in his lab and under his supervision. Finally, I would like to thank the Putnman Laboratory for allowing me to use their equipment and Dr. Susan C. Pannullo for introducing me to Dr. Shuler and their joint project, which I became apart of.

APPENDIX A – Library of Hydrogels

Sample	Code	Date of synthesis	Date of GPC	Mn	Mw	PDI	Mn by NMR
PCL-PEG-PCL 2,000-2,000-2,000	AT1	03-05-10	05-04-10				
PCL-PEG-PCL 1,000-1,000-1,000	AT2	03-16-10	05-04-10	6371	7720	1.21	
PCL-PEG-PCL 2,000-2,000-2,000	AT3	03-18-10	05-04-10	6263	8152	1.30	
PCL-PEG-PCL 1,000-1,000-1,000	AT4	04-20-10	05-06-10	4058	4822	1.18	
PCL-PEG-PCL 1,000-1,000-1,000	AT5	04-27-10	05-06-10	6303	8003	1.27	
PCL-PEG-PCL 750-1,000-750	AT6	04-27-10	05-06-10	3457	4284	1.23	
PLGA-PEG-PLGA 2,000-2,000-2,000	AT7	03-22-10	05-07-10	6291	8254	1.31	
PLGA-PCL-PEG-PCL-PLGA 1,000-1,000-2,000-1,000-1,000	AT8	03-21-10 04-01-10	05-07-10	7834	8897	1.14	
PLGA-PCL-PEG-PCL-PLGA 500-500-1,000-500-500	AT9	03-21-10 04-01-10	05-07-10	3623	4038	1.11	
PCL-PLGA-PEG-PLGA-PCL 1,000-1,000-2,000-1,000-1,000	AT10	03-22-10 04-10-10	05-07-10	7420	9279	1.25	
PLGA-PEG-PLGA 1,000-1,000-1,000 (1:1, L-lactide/glycolide)	AT11	04-10-10	05-07-10	3203	3993	1.25	2978
PLGA-PEG-PLGA 1,000-1,000-1,000 (3:1, L-lactide/glycolide)	AT12	05-22-10	06-08-10	2149	2557	1.19	
PLGA-PEG-PLGA 1,000-1,000-1,000 (3:1, L-lactide/glycolide)	AT13	05-22-10	06-08-10	2220	2617	1.18	
PCLA-PEG-PCLA 1,000-1,000-1,000	AT14	05-27-10	06-08-10	2937	3456	1.18	
PCLA-PEG-PCLA 1,000-1,000-1,000	AT15	05-29-10	06-08-10	2842	3337	1.17	
PLGA-PEG-PLGA 1,000-1,000-1,000 (3:1, DL-lactide/glycolide)	AT16	05-20-10 06-11-10	06-08-10	2026	2383	1.18	
PLGA-PEG-PLGA 1,500-1,000-1,500 (3:1, DL-lactide/glycolide)	AT17		06-14-10	4815	6147	1.28	
PCL-PEG-PCL 7,000-1,000-7,000	AT18	06-11-10	06-14-10	3190	4051	1.29	
PLGA-PEG-PLGA 1,000-1,000-1,000 (3:1, DL-lactide/glycolide)	AT19	06-16-10	06-17-10	3280	3690	1.13	2948
PLGA-PEG-PLGA 1,200-1,000-1,200 (3:1, DL-lactide/glycolide)	AT20	06-30-10	07-02-10	2608	2943	1.13	
PLGA-PEG-PLGA 1,250-1,000-1,250 (3:1, DL-lactide/glycolide)	AT21	07-28-10	09-08-10	3075	3688	1.20	3260
PLGA-PEG-PLGA 1,250-1,000-1,250 (1:1, L-lactide/glycolide)	AT22	07-28-10	08-02-10	2714	3326	1.23	
PLGA-PEG-PLGA 1,250-1,000-1,250 (3:1, DL-lactide/glycolide)	AT23	08-04-10	09-08-10	2531	2760	1.09	2760
PLGA-PEG-PLGA 1,000-1,000-1,000 (1:1, L-lactide/glycolide)	AT24	08-04-10	09-08-10	3366	4100	1.22	3730
PLGA-PEG-PLGA 1,000-1,000-1,000 (1:1, L-lactide/glycolide)	AT25	08-06-10	09-08-10	2833	3376	1.19	3000

APPENDIX B – Release Curves of Congo Red

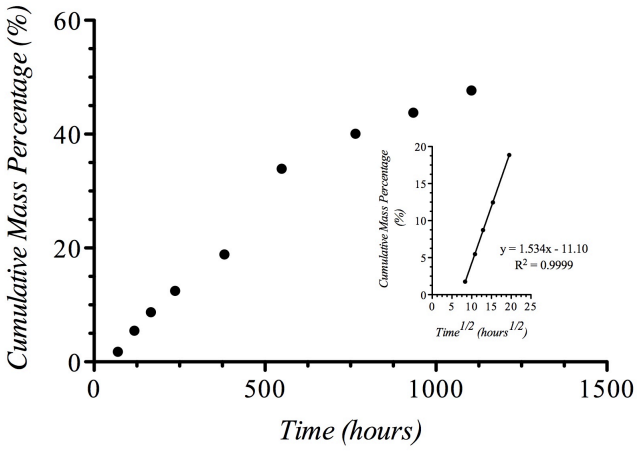

A

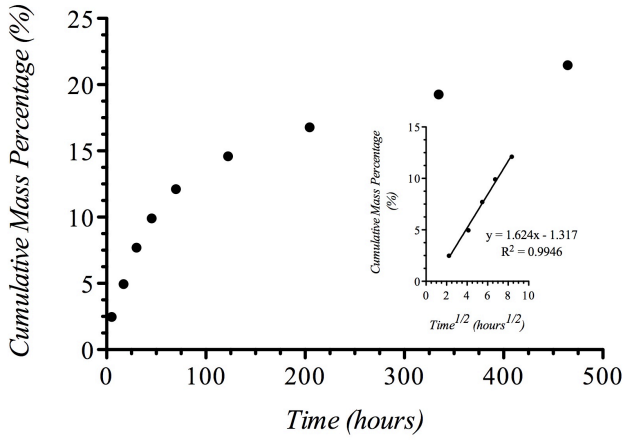

B

A) The release profile of Congo Red at room temperature. B) The release profile at 37°C.

References

[1] K.R. Hess, K.R. Broglio, M.L. Bondy, Adult glioma incidence trends in the United States, 1977-2000. Cancer 101(10) (2004) 2293-2299.

[2] C.J. Wikstrand, R.E. McLendon, A.H. Friedman, D.D. Bigner, Cell surface localization and density of the tumor-associated variant of the epidermal growth factor receptor, EGFRvIII. Cancer Res 57(18) (1997) 4130-4140.

[3] J.A. McCubrey, M.M. Lahair, R.A. Franklin, OSU-03012 in the treatment of glioblastoma. Mol Pharmacol 70(2) (2006) 437-439.

[4] K.E. Wallner, J.H. Galicich, G. Krol, E. Arbit, M.G. Malkin, Patterns of failure following treatment for glioblastoma multiforme and anaplastic astrocytoma. Int J Radiat Oncol Biol Phys 16(6) (1989) 1405-1409.

[5] M. Salcman, Survival in glioblastoma: historical perspective. Neurosurgery 7(5) (1980) 435-439.

[6] M. Lacroix, D. Abi-Said, D.R. Fourney, Z.L. Gokaslan, W. Shi, F. DeMonte, F.F. Lang, I.E. McCutcheon, S.J. Hassenbusch, E. Holland, K. Hess, C. Michael, D. Miller, R. Sawaya, A multivariate analysis of 416 patients with glioblastoma multiforme: prognosis, extent of resection, and survival. J Neurosurg 95(2) (2001) 190-198.

[7] M. Ammirati, N. Vick, Y.L. Liao, I. Ciric, M. Mikhael, Effect of the extent of surgical resection on survival and quality of life in patients with supratentorial glioblastomas and anaplastic astrocytomas. Neurosurgery 21(2) (1987) 201-206.

[8] P.C. Burger, S.B. Green, Patient age, histologic features, and length of survival in patients with glioblastoma multiforme. Cancer 59(9) (1987) 1617-1625.

[9] Prognostic factors for high-grade malignant glioma: development of a prognostic index. A Report of the Medical Research Council Brain Tumour Working Party. J Neurooncol 9(1) (1990) 47-55.

[10] M.G. Donelli, M. Zucchetti, M. D'Incalci, Do anticancer agents reach the tumor target in the human brain? Cancer Chemother Pharmacol 30(4) (1992) 251-260.

[11] J.F. Deeken, W. Loscher, The blood-brain barrier and cancer: transporters, treatment, and Trojan horses. Clin Cancer Res 13(6) (2007) 1663-1674.

[12] K.W. Li, W. Dang, B.M. Tyler, G. Troiano, T. Tihan, H. Brem, K.A. Walter, Polilactofate microspheres for Paclitaxel delivery to central nervous system malignancies. Clin Cancer Res 9(9) (2003) 3441-3447.

[13] P. Sampath, H. Brem, Implantable Slow-Release Chemotherapeutic Polymers for the Treatment of Malignant Brain Tumors. Cancer Control 5(2) (1998) 130-137.

[14] L.K. Fung, M. Shin, B. Tyler, H. Brem, W.M. Saltzman, Chemotherapeutic drugs released from polymers: distribution of 1,3-bis(2-chloroethyl)-1-nitrosourea in the rat brain. Pharm Res 13(5) (1996) 671-682.

[15] C. Guerin, A. Olivi, J.D. Weingart, H.C. Lawson, H. Brem, Recent advances in brain tumor therapy: local intracerebral drug delivery by polymers. Invest New Drugs 22(1) (2004) 27-37.

[16] L.K. Fung, M.G. Ewend, A. Sills, E.P. Sipos, R. Thompson, M. Watts, O.M. Colvin, H. Brem, W.M. Saltzman, Pharmacokinetics of interstitial delivery of carmustine, 4-hydroperoxycyclophosphamide, and paclitaxel from a biodegradable polymer implant in the monkey brain. Cancer Res 58(4) (1998) 672-684.

[17] A. Giese, M. Westphal, Glioma invasion in the central nervous system. Neurosurgery 39(2) (1996) 235-250; discussion 250-232.
[18] F.H. Hochberg, A. Pruitt, Assumptions in the radiotherapy of glioblastoma. Neurology 30(9) (1980) 907-911.
[19] W.M.S. Lawrence K. Fung, Polymeric implants for cancer chemotherapy. Advanced Drug Delivery Reviews 26(2-3) (1997) 21.
[20] E.K. Rowinsky, R.C. Donehower, Paclitaxel (taxol). N Engl J Med 332(15) (1995) 1004-1014.
[21] B.Y. Ong, S.H. Ranganath, L.Y. Lee, F. Lu, H.S. Lee, N.V. Sahinidis, C.H. Wang, Paclitaxel delivery from PLGA foams for controlled release in post-surgical chemotherapy against glioblastoma multiforme. Biomaterials 30(18) (2009) 3189-3196.
[22] P. Kumar Naraharisetti, B. Yung Sheng Ong, J. Wei Xie, T. Kam Yiu Lee, C.H. Wang, N.V. Sahinidis, In vivo performance of implantable biodegradable preparations delivering Paclitaxel and Etanidazole for the treatment of glioma. Biomaterials 28(5) (2007) 886-894.
[23] N.L. Elstad, K.D. Fowers, OncoGel (ReGel/paclitaxel)--clinical applications for a novel paclitaxel delivery system. Adv Drug Deliv Rev 61(10) (2009) 785-794.
[24] J.L. XJ Loh, Biodegradable thermosensitive copolymer hydrogels for drug delivery. Expert Opinion on Therapeutic Patents 17 (2007) 8.
[25] T. Arai, T. Joki, M. Akiyama, M. Agawa, Y. Mori, H. Yoshioka, T. Abe, Novel drug delivery system using thermoreversible gelation polymer for malignant glioma. J Neurooncol 77(1) (2006) 9-15.
[26] T. Ozeki, K. Hashizawa, D. Kaneko, Y. Imai, H. Okada, Treatment of rat brain tumors using sustained-release of camptothecin from poly(lactic-co-glycolic acid) microspheres in a thermoreversible hydrogel. Chem Pharm Bull (Tokyo) 58(9) 1142-1147.
[27] U. Akbar, T. Jones, J. Winestone, M. Michael, A. Shukla, Y. Sun, C. Duntsch, Delivery of temozolomide to the tumor bed via biodegradable gel matrices in a novel model of intracranial glioma with resection. J Neurooncol 94(2) (2009) 203-212.
[28] B. Tyler, K.D. Fowers, K.W. Li, V.R. Recinos, J.M. Caplan, A. Hdeib, R. Grossman, L. Basaldella, K. Bekelis, G. Pradilla, F. Legnani, H. Brem, A thermal gel depot for local delivery of paclitaxel to treat experimental brain tumors in rats. J Neurosurg 113(2) 210-217.
[29] G.M. Zentner, R. Rathi, C. Shih, J.C. McRea, M.H. Seo, H. Oh, B.G. Rhee, J. Mestecky, Z. Moldoveanu, M. Morgan, S. Weitman, Biodegradable block copolymers for delivery of proteins and water-insoluble drugs. J Control Release 72(1-3) (2001) 203-215.
[30] H.H. Ginary, K. Wong, K. Lai, BRAIN PHANTOM PROJECT: Master of Engineering Design Project. Cornell University (2007).
[31] Z.J. Chen, G.T. Gillies, W.C. Broaddus, S.S. Prabhu, H. Fillmore, R.M. Mitchell, F.D. Corwin, P.P. Fatouros, A realistic brain tissue phantom for intraparenchymal infusion studies. J Neurosurg 101(2) (2004) 314-322.
[32] A. Torress, C. Zhu, Susan Panullo, Michael Shuler, Paclitaxel delivery to brain tumors from hydrogels: a computational study. Biotechnology Progress (2011).(Under revision)

[33] D.Y. Arifin, K.Y. Lee, C.H. Wang, K.A. Smith, Role of convective flow in carmustine delivery to a brain tumor. Pharm Res 26(10) (2009) 2289-2302.
[34] C.C. Wang, J. Li, C.S. Teo, T. Lee, The delivery of BCNU to brain tumors. J Control Release 61(1-2) (1999) 21-41.
[35] S.J.C. MR, Targeted drug delivery for treatment and imaging of glioblastoma multiforme. Expert Opinion on Drug Delivery 6(7) (2009) 705-718.
[36] J.A. Boockvar, A.J. Tsiouris, C.P. Hofstetter, I. Kovanlikaya, S. Fralin, K. Kesavabhotla, S.M. Seedial, S.C. Pannullo, T.H. Schwartz, P. Stieg, R.D. Zimmerman, J. Knopman, R.J. Scheff, P. Christos, S. Vallabhajosula, H.A. Riina, Safety and maximum tolerated dose of superselective intraarterial cerebral infusion of bevacizumab after osmotic blood-brain barrier disruption for recurrent malignant glioma. J Neurosurg 114(3) 624-632.
[37] S. Dey, P.M. Spring, S. Arnold, J. Valentino, D. Chendil, W.F. Regine, M. Mohiuddin, M.M. Ahmed, Low-dose fractionated radiation potentiates the effects of Paclitaxel in wild-type and mutant p53 head and neck tumor cell lines. Clin Cancer Res 9(4) (2003) 1557-1565.
[38] C. He, S.W. Kim, D.S. Lee, In situ gelling stimuli-sensitive block copolymer hydrogels for drug delivery. J Control Release 127(3) (2008) 189-207.
[39] R.V. La Rocca, H.M. Mehdorn, Localized BCNU chemotherapy and the multimodal management of malignant glioma. Curr Med Res Opin 25(1) (2009) 149-160.
[40] A. Narayana, P. Kelly, J. Golfinos, E. Parker, G. Johnson, E. Knopp, D. Zagzag, I. Fischer, S. Raza, P. Medabalmi, P. Eagan, M.L. Gruber, Antiangiogenic therapy using bevacizumab in recurrent high-grade glioma: impact on local control and patient survival. J Neurosurg 110(1) (2009) 173-180.